



## Use of Underpotential Deposition for Evaluation of Overpotential Deposition Kinetics of Reactive Metals

E. Guerra,<sup>a,\*</sup> G. H. Kelsall,<sup>a,\*\*,c</sup> M. Bestetti,<sup>a,d</sup> D. Dreisinger,<sup>a</sup> K. Wong,<sup>b</sup>  
K. A. R. Mitchell,<sup>b</sup> and D. Bizzotto<sup>b,\*\*,z</sup>

<sup>a</sup>Department of Metals and Materials Engineering, and <sup>b</sup>Department of Chemistry, Advanced Materials Process Engineering Laboratory, University of British Columbia, Vancouver, British Columbia V6T 1Z4, Canada

The underpotential deposition (UPD) of Zn onto Pt is shown to produce an electrode surface which is suitable for the evaluation of Zn overpotential kinetics. The UPD of Zn onto polycrystalline Pt was characterized in acidic and neutral sulfate solutions using voltammetric charge measurements and X-ray photoelectron spectroscopy. The charge density for UPD Zn deposition on platinum from neutral sulfate solution was estimated to be  $260 \pm 30 \mu\text{C cm}^{-2}$ , consistent with a monolayer. The decrease in H<sub>2</sub> evolution rates provided further evidence of the formation of a Zn UPD layer. Evidence for the formation of a Zn-Pt alloy, resulting from polarization of the Pt electrode at a potential between the Zn UPD and overpotential deposition potentials is also presented. The alloy was oxidized at the same potential as the Pt substrate, illustrating the large interaction between Zn and Pt due to the small crystallographic misfit. The alloy also decreased H<sub>2</sub> evolution rates, relative to the Pt substrate. The use of such a modified substrate for measurement of kinetic parameters for metal deposition is described and the results obtained are shown to compare favorably with the literature values.

© 2003 The Electrochemical Society. [DOI: 10.1149/1.1631282] All rights reserved.

Manuscript received April 26, 2003. Available electronically November 21, 2003.

The extended Butler-Volmer equation is often invoked to model the relationship between current density and overpotential for electrochemical reactions. However, the equation is based on the assumption that the electrode is a smooth planar surface with a corresponding uniform potential distribution. The extended Butler-Volmer equation for electrodeposition of a metal, Me, including a provision for electrode roughness is

$$j_{\text{Me}} = \frac{-j_{0,\text{Me}} \left[ e^{\frac{-\xi \alpha n F \eta_{\text{Me}}}{RT}} - e^{\frac{\xi (1-\alpha) n F \eta_{\text{Me}}}{RT}} \right]}{1 - \frac{j_{0,\text{Me}}}{j_{\text{lim,Me}}} e^{\frac{-\xi \alpha n F \eta_{\text{Me}}}{RT}}} \quad [1]$$

where  $j_{\text{Me}}$  (A m<sup>-2</sup>) is the current density of the metal deposition reaction,  $j_{0,\text{Me}}$  (A m<sup>-2</sup>) is the exchange current density,  $\eta_{\text{Me}}$  is the overpotential,  $\alpha$  is the transfer coefficient,  $n$  is the number of electrons transferred in the rate-determining step, and  $\xi$  is the power term of the double-layer capacitance ( $\xi = 1.0$  for a perfectly smooth electrode and  $\xi = 0.5$  for a porous electrode). By inspection, the Tafel slope for a reaction occurring on an extremely rough electrode, which is analogous to a porous electrode, should be double that of an otherwise identical smooth electrode.<sup>1</sup>

When studying the kinetics of overpotential deposition, OPD, of a metal the natural desire is to construct the electrode using the metal of interest. However, many industrially important metals are soft and reactive, which makes it difficult to reproducibly prepare pristine electrodes, particularly single-crystal electrodes. In addition, the growth of metal deposits, particularly at high current density, can significantly alter the morphology and surface area of the electrode on which they occur. During subsequent polarization experiments the hysteresis in the response of the electrode resulting from the deposition of rough or dendritic deposits requires that the electrode be extracted from the electrolytic cell and repolished after each use. The underpotential deposition (UPD) of a reactive metal on a noble

foreign substrate, S, is proposed as a general technique for generating suitable electrode surfaces for the study of OPD kinetics, using the Zn-Pt system as a model case.

*Underpotential deposition.*—In general, underpotential deposition describes the formation of a two-dimensional layer of metal, Me, onto a foreign substrate, S, at a potential more positive than that for bulk deposition of the metal. In the absence of UPD layer formation, or in cases where UPD results in a significant crystallographic misfit between the depositing metal and the substrate, overpotential deposition of the metal over the substrate is heterogeneous. However, if a Me-S UPD system can be selected such that the degree of crystallographic misfit is small, then OPD of the metal over the UPD covered substrate should be homogeneous and progress epitaxially at low current densities. Thus, the crystallographic orientation and surface area of the OPD Me can be taken to be the same as the original surface of the substrate. Therefore, the current density-overpotential relationship for bulk deposition of the metal can be mapped by first coating the substrate at low overpotential and then pulsing to a potential in the region of bulk deposition, until a steady-state current response results. In between pulses, the potential can be returned to a value between the UPD Me and OPD Me potentials, thereby stripping away the bulk metal from the electrode surface and recovering the original geometry and crystallographic orientation of the UPD-coated electrode surface. OPD metal deposition on UPD modified substrates has been widely reported and the more general literature on electrochemical phase formation and growth reviewed, including growth on UPD modified substrates.<sup>2,3</sup> The identification of a particular Me-S UPD system can be accomplished experimentally, using standard electrochemical techniques, or predicted from theoretical calculations.<sup>4,5</sup>

*UPD of zinc on platinum.*—The potential for Zn UPD onto Pt, ca.  $-0.25$  V vs. SCE, was identified and studied by Aramata *et al.*<sup>6-13</sup> The potential shift for Zn UPD on platinum, *i.e.*, the potential difference between bulk Zn deposition and UPD deposition, ranges from 1.04 to 1.19 V.<sup>7</sup> The relatively small variations in the UPD potential shift in different electrolytes have been attributed to the effects of different adsorbed species over the UPD layer.

By applying relatively low overpotential pulses for extended times, Despić and Pavlović<sup>14</sup> found that the corresponding zinc deposition current response was independent of time. This demonstrated that the real surface area of the electrode was independent of time, suggesting two-dimensional layer-by-layer growth of the zinc deposit. This result was consistent with the calculated crystallo-

\* Electrochemical Society Student Member.

\*\* Electrochemical Society Active Member.

<sup>c</sup> Present address: Department of Chemical Engineering and Chemical Technology, Imperial College, London SW7 2BY, United Kingdom.

<sup>d</sup> Present address: Department of Chemistry, Materials and Chemical Engineering, Polytechnic of Milan, 20131 Milan, Italy.

<sup>z</sup> E-mail: bizzotto@chem.ubc.ca

graphic Pt-Zn misfit. The misfit ( $f$ ) is calculated from the interatomic distances ( $d$ ) between Zn-Zn, 2.665 Å, and Pt-Pt, 2.775 Å

$$f = \frac{d_{0,\text{Zn}} - d_{0,\text{Pt}}}{d_{0,\text{Pt}}} = \frac{2.665 - 2.775}{2.775} = -0.04 \quad [2]$$

The relatively small negative value of the crystallographic misfit suggests that, in the absence of specifically adsorbed anions, zinc can fully occupy interstitial sites on the platinum surface. Characterization of the UPD and alloy surface of the Pt-Zn system are presented, including an example demonstrating the utility of such a modified surface for kinetic measurements of reactive metal reduction.

### Experimental

The underpotential deposition of zinc on polycrystalline platinum from deoxygenated sulfuric acid and neutral magnesium sulfate solutions was studied by cyclic voltammetry using a jacketed three-compartment electrochemical cell with a saturated calomel (SCE) reference electrode under a nitrogen atmosphere. The temperature was controlled using a refrigerated circulating bath (Fisher Scientific Isotemp model 900). The electrode employed was a model MTI34 (99.99+ %) platinum ring-disk electrode (RDE, Pine Instrument Co.) with a disk area of 0.283 cm<sup>2</sup>. The disk surface was polished to a mirror finish using 1 μm diamond slurry. The potentiostat was an Eco-Chemie PSTAT 30, equipped with BIPOT, FRA and SCAN-GEN modules. The zinc solutions were prepared using aliquots of a strong, 2 mol dm<sup>-3</sup>, zinc sulfate solution, which was prepared from ACS grade zinc sulfate heptahydrate, ZnSO<sub>4</sub>·7H<sub>2</sub>O (Fluka) and Millipore Milli-Q ultrapure water (18 MΩ cm). Impurities were reduced from the concentrated zinc solution using a platinum flag electrode, polarized at -1.0 V vs. SCE for approximately 6 h while the solution was stirred vigorously under a nitrogen atmosphere. The sulfuric acid and magnesium sulfate (Fisher Scientific) employed were ACS grade reagents.

Zinc overpotential deposition was studied by cyclic, normal pulse, and staircase voltammetry from pure zinc sulfate electrolytes using the same equipment and reagents as described above. The normal pulse and staircase voltammetry experiments employed a base potential of -0.25 V vs. SCE and were repeated three times at each of three electrode rotation speeds, 400, 1600, and 3600 rpm. The applied potentials were corrected for ohmic drop after the experiment by estimating the solution resistance using electrochemical impedance spectroscopy at -0.25 V vs. SCE, after all deposited Zn had been stripped at this potential. The real and imaginary components of the complex impedance,  $Z$ , were measured during application of a 10 mV rms perturbation in a sine wave format in the frequency range of 100 to 1000 Hz. The frequency response was modeled as a series resistor-constant phase element,  $CPE$ , circuit according to the equation below

$$Z = R_{\text{soln}} + (i\omega CPE)^{-\xi} \quad [3]$$

X-ray photoelectron spectroscopy (XPS) analyses were performed using a Leybold MAX200 spectrometer with a Mg Kα source (1253.6 eV) operated at 15 kV, 20 mA, and a system pressure of  $1 \times 10^{-9}$  mbar. Spectra were obtained with a pass energy of 48 eV. Binding energies were referenced to the Au 4f<sub>1/2</sub> peak at 84.0 eV.

### Results

**Behavior in sulfuric acid supporting electrolyte.**—Voltammograms for the Pt with and without  $10^{-4}$  mol dm<sup>-3</sup> ZnSO<sub>4</sub> in 0.1 mol dm<sup>-3</sup> H<sub>2</sub>SO<sub>4</sub> are shown in Fig. 1. The voltammograms are similar to those reported by Aramata *et al.*<sup>6</sup> The features identified are the onset of UPD Zn formation, I at ca. 0 V vs. SCE, H<sub>2</sub> evolution, II at ca. -0.25 V, and stripping of UPD Zn, III at ca. -0.2 V vs. SCE; the formation and stripping of the UPD Zn layer appeared to be quite reversible. However, as illustrated in Fig. 2, when

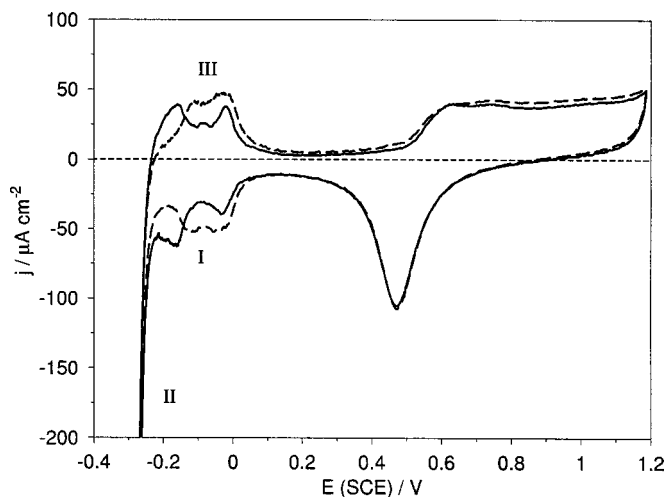


**Figure 1.** Cyclic voltammograms of polycrystalline platinum in 0.1 M H<sub>2</sub>SO<sub>4</sub>, pH 0.7, with (— — —) and without (—) 0.001 M ZnSO<sub>4</sub> at 25°C, scan rate 20 mV s<sup>-1</sup>, 1600 rpm electrode rotation speed.

the electrode was conditioned at a potential in the Zn UPD potential region, -0.2 V vs. SCE in this case, the stripping current of the UPD Zn layer, III, diminished, possibly due to formation of a 2D surface alloy by a site exchange process. Tadjeddine *et al.*<sup>15</sup> has described alloy formation during Zn UPD on Au and surface alloy formation resulting from such polarization routines has been reported for several UPD systems including Pb-Au,<sup>16,17</sup> Pb-Ag,<sup>17</sup> Cd-Ag,<sup>18</sup> Cd-Au,<sup>19,20</sup> Tl-Ag,<sup>21</sup> and Sn-Au.<sup>22</sup> Despić and Pavlović,<sup>14</sup> in fact, had previously described Zn UPD and rapid alloy formation commencing at ca. -0.8 V vs. SCE, which was reported as the UPD potential in 1.5 M ZnSO<sub>4</sub> buffered at pH 3.5, from which some zinc was released from the platinum substrate only as it was oxidized (IV in Fig. 2). Electroplating of zinc onto platinum from sulfate solution has long been determined to result in the formation of a 3D 1:1 Zn-Pt surface alloy.<sup>23</sup> The formation of this alloy is so rapid as to be visible to the naked eye after only 15 min of zinc deposition, which is reflected in the relatively large diffusion coefficient of Zn into Pt at 100°C;  $5.0 \times 10^{-15}$  cm<sup>2</sup> s<sup>-1</sup> (ca. 10<sup>7</sup> times greater than the diffusion coefficient of Zn into Cu).<sup>23</sup> The 3D alloy resulting from bulk

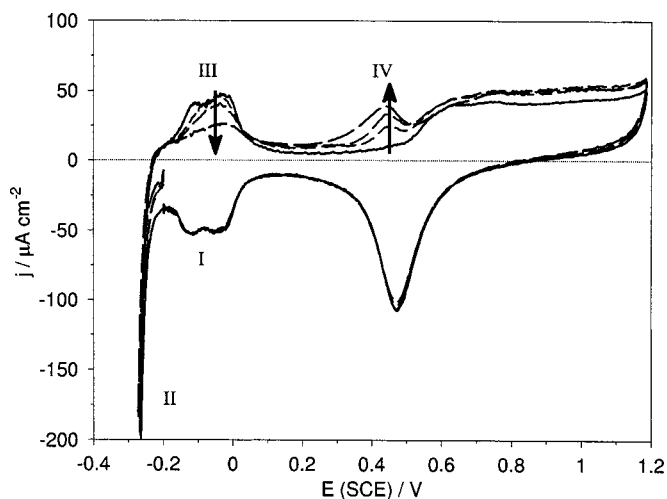


**Figure 2.** Cyclic voltammograms of polycrystalline platinum in 0.1 M H<sub>2</sub>SO<sub>4</sub>, pH 0.7, with 0.001 M ZnSO<sub>4</sub> at 25°C, scan rate 20 mV s<sup>-1</sup>, 0.9 V vs. SCE rest potential, 1600 rpm electrode rotation speed, as a function of conditioning time at -0.200 V vs. SCE, 0 s (—), 900 s (- - -), 1800 s (- · - ·), 3600 s (- - -).

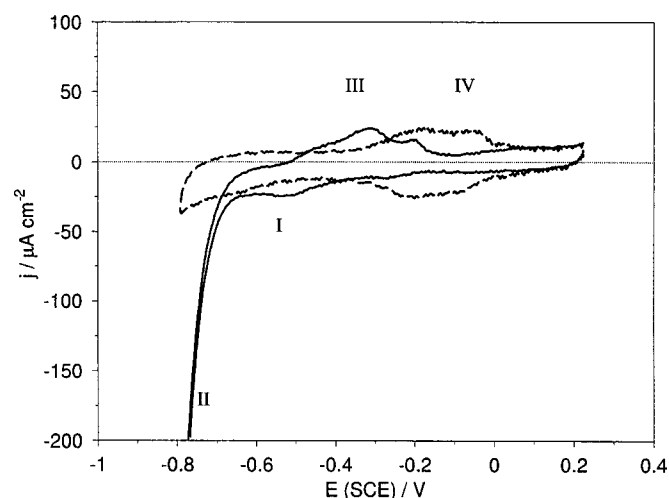


**Figure 3.** Cyclic voltammograms of polycrystalline platinum in 0.1 M  $\text{MgSO}_4$ , with (—) and without (---) 0.0001 M  $\text{ZnSO}_4$ , pH 5.8, at 25°C, scan rate 20  $\text{mV s}^{-1}$ , 1600 rpm electrode rotation speed.

zinc deposition cannot be removed with hot nitric or hot hydrochloric acid, but can be removed using aqua regia (which would have also dissolved the platinum substrate).<sup>23</sup> The implication is that the 2D surface alloy formed in the UPD region has chemical properties similar to the bulk 3D alloy.

In a strongly acidic sulfate electrolyte, see Fig. 2, the suppression of the hydrogen evolution rate was barely evident. Aramata *et al.*<sup>11</sup> have described a shift in the onset of Zn UPD on Pt(111) towards more negative potentials with decreasing pH in a phosphate supporting electrolyte, which was attributed to stronger adsorption of phosphate species at lower pHs.<sup>11</sup> Though this effect was reportedly absent in sulfate media, the conclusion was based on interpretations of cyclic voltammograms in the pH range of 0.8 to 3.7.<sup>12</sup> At pH < 3.3 and in the potential range of sulfate/bisulfate adsorption on Pt(111), bisulfate is the predominantly adsorbed species while sulfate is the prevalent at pH > 4.7.<sup>24</sup> Thus, it is reasonable to assume that at pHs  $\leq 3.7$ , bisulfate anions may block Zn UPD on certain regions of the Pt electrode. When the potential was swept into the region of hydrogen evolution the electrode areas which were not occupied by Zn would have catalyzed hydrogen evolution, which accounts for the lack of significant inhibition of hydrogen evolution at low pH.

The integration of the charge for the Zn UPD layer, required for the estimation of the degree of coverage of the platinum, is difficult because, at this pH, Zn UPD also occurs in the same potential region as hydrogen adsorption, and it is not clear to what extent Zn UPD forms preferentially with respect to hydrogen adsorption.

**Behavior in magnesium sulfate supporting electrolyte.**—Experiments were conducted in neutral magnesium sulfate solution to maximize the surface coverage of UPD Zn and to separate the regions of UPD Zn and hydrogen adsorption on Pt. As illustrated in Fig. 3, the potential region of hydrogen adsorption, I, was shifted to a more negative potential, *ca.*  $-0.4$  V vs. SCE, together with bulk hydrogen evolution, II, which then occurred at *ca.*  $-0.8$  V vs. SCE, and oxidation of adsorbed hydrogen, III, at between *ca.*  $-0.5$  to  $-0.2$  V vs. SCE. After the addition of  $10^{-4}$  mol  $\text{dm}^{-3}$  zinc sulfate, the potential region of Zn UPD, IV, between *ca.*  $-0.4$  and 0 V vs. SCE, appears clearly separate from hydrogen adsorption. The potential range for Zn UPD and the shape of the voltammogram appear quite similar to Zn UPD on polycrystalline Pt from 0.1 mol  $\text{dm}^{-3}$   $\text{KH}_2\text{PO}_3$  buffered at pH 5.9.<sup>6</sup>

The charge density for Zn UPD formation was estimated to be  $260 \pm 30$   $\mu\text{C cm}^{-2}$  determined by integrating the current response (Fig. 4) to a potential pulses between 0.2 to  $-0.4$  V vs. SCE at

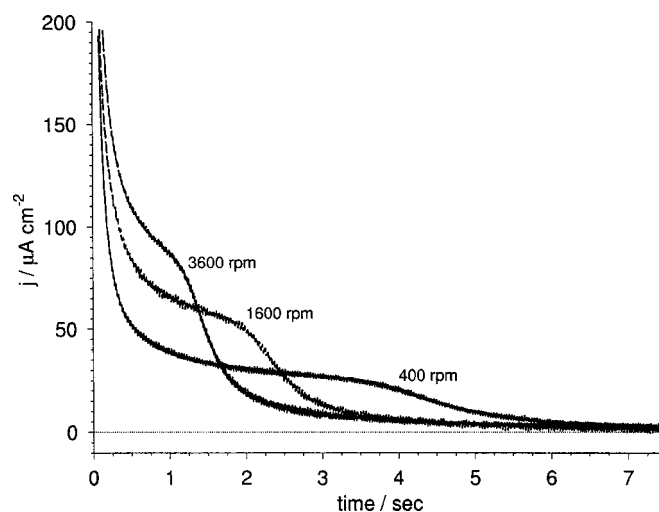


**Figure 4.** Current density response of polycrystalline platinum in 0.1 M  $\text{MgSO}_4$  with 0.0001 M  $\text{ZnSO}_4$  pH 5.8, at 25°C, to a potential pulse from 0.2 to  $-0.4$  V vs. SCE, as a function of electrode rotation speed.

electrode rotation speeds of 400, 1600, and 3600 rpm. During the initial stages of the pulses, the currents were determined to vary directly with the square root of time, which is typical of semi-infinite linear diffusion during relaxation of the boundary layer. The plateaus in current responses, which tended to zero at Zn-filled sites on the Pt surface, were consistent with the mass-transport control of  $\text{Zn}^{2+}$  coupled with rapid heterogeneous UPD.<sup>25</sup> Zn UPD on polycrystalline Pt is reportedly similar to that on Pt(110) (the facet on which Zn UPD occurs to the greatest extent).<sup>11</sup> The calculated charge density for the Zn UPD value is somewhat smaller than the figure of  $320$   $\mu\text{C cm}^{-2}$  reported for Zn UPD formation on Pt(110) in 0.1 mol  $\text{dm}^{-3}$   $\text{KH}_2\text{PO}_4$  at pH 3.7.<sup>11</sup> However,  $260$   $\mu\text{C cm}^{-2}$  is not unreasonable when considering that the theoretical charge densities for full coverage of Zn on Pt(110) is  $294$   $\mu\text{C cm}^{-2}$ .

In order to ensure that the calculated charge density was not overestimated, the polished platinum electrode was characterized using atomic force microscopy (AFM). By simply calculating the sum of the areas of triangles between all groups of three adjacent points in the array of  $z$  position data, the real surface area of the electrode was estimated to be was only approximately 0.4% greater than the geometric area.

A notable feature of the presence of a Zn UPD layer on Pt is its dramatic effect on hydrogen evolution kinetics, as illustrated in Fig. 5. Even at relatively large overpotentials, *e.g.*, 0.3 V corresponding to *ca.*  $-1.1$  V vs. SCE, at which zinc bulk deposition occurs, the corresponding hydrogen evolution current density was close to that observed in the absence of zinc at *ca.*  $-0.8$  V. Normally, hydrogen evolution on platinum at such a high overpotential would be excessive and result in the electrode surface becoming covered in hydrogen gas bubbles. The presence of the UPD Zn layer on platinum, though clearly not to the same extent as pure zinc, has some enhanced property of inhibiting hydrogen evolution compared to bare platinum. It is likely that the relatively neutral pH of the magnesium sulfate solution is related to increased coverage by the zinc UPD layer. Mascaro-Lucia *et al.*<sup>26</sup> have described a strong inhibition of hydrogen evolution due to increased coverage of Zn UPD on polycrystalline Pt in acidic fluoride media relative to acidic sulfate media, for which corresponding stripping charges of the Zn UPD layer were 350 and 210  $\mu\text{C cm}^{-2}$ , respectively. From this observation it was concluded that adsorbed sulfate or bisulfate partially blocked Zn UPD in acidic sulfate electrolytes and that  $350$   $\mu\text{C cm}^{-2}$  was closer to the value for complete coverage of the Pt electrode by UPD Zn. The implication is that for bulk deposition experiments from sulfate-based electrolytes, a Zn UPD modified platinum electrode

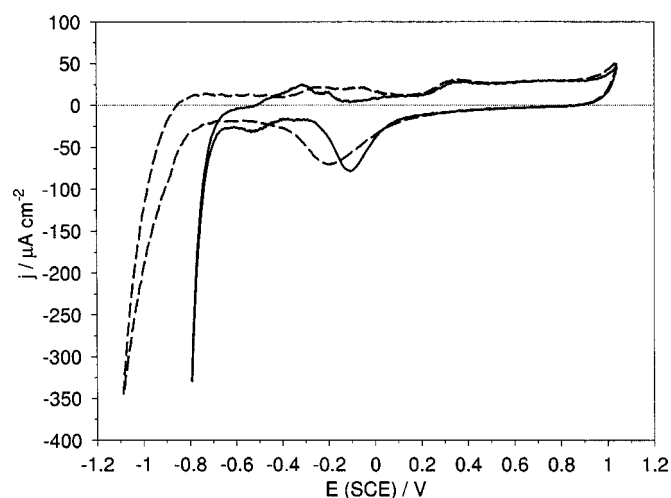


**Figure 5.** Cyclic voltammetry on polycrystalline platinum in 0.1 M  $\text{ZnSO}_4$ , pH 4.9 at 25°C, scan rate 20  $\text{mV s}^{-1}$ , 1600 rpm electrode rotation rate.

should be prepared in a near-neutral solution. This diminishes the reversible potential and hence the kinetics of hydrogen adsorption and/or bisulfate adsorption, thereby biasing the competitive adsorption on Pt in favor of Zn. The upper pH limit is dictated by the ultimate precipitation of  $\text{Zn(OH)}_2$ .

**Voltammetry in aqueous zinc sulfate electrolyte solutions.**—In order to reproduce the surface alloy formed in sulfuric acid supporting electrolyte, pH 0.7 (Fig. 2), the electrode was polarized for various times at  $-0.4 \text{ V vs. SCE}$  in 0.1  $\text{mol dm}^{-3}$   $\text{ZnSO}_4$ , pH 4.9, which is slightly more positive than potentials at which hydrogen evolution occurs. As illustrated in Fig. 6, when the potential was swept towards more positive potentials, the stripping current in the UPD Zn region decreased as waiting time increased, indicated by the down arrow, while current in the region of platinum oxidation increased, indicated by the up arrow. The effect was limited to approximately the first 600 s of conditioning, which was interpreted as the time for transformation of the UPD layer to a surface alloy. However, although the possibility is not excluded, it is not claimed that the entire UPD layer was transformed to an alloy, only that whatever fraction of the surface which would have undergone a site

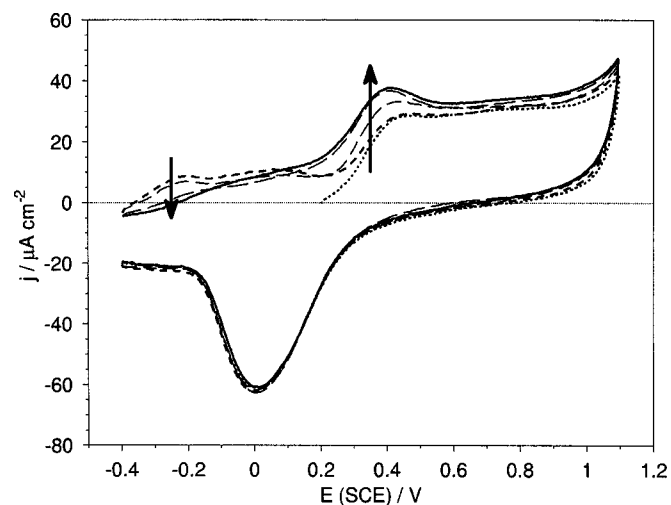


**Figure 6.** Sweep voltammetry of polycrystalline platinum in 0.1 M  $\text{ZnSO}_4$ , pH 4.9 at 25°C, scan rate 20  $\text{mV s}^{-1}$ , 1600 rpm electrode rotation rate, as a function of waiting time at  $-0.4 \text{ V vs. SCE}$ , 0 s (---), 120 s (— — —), 600 s (— · — · —), 1200 s (— — —) and at 0.2 V vs. SCE 600 s (· · · · ·).

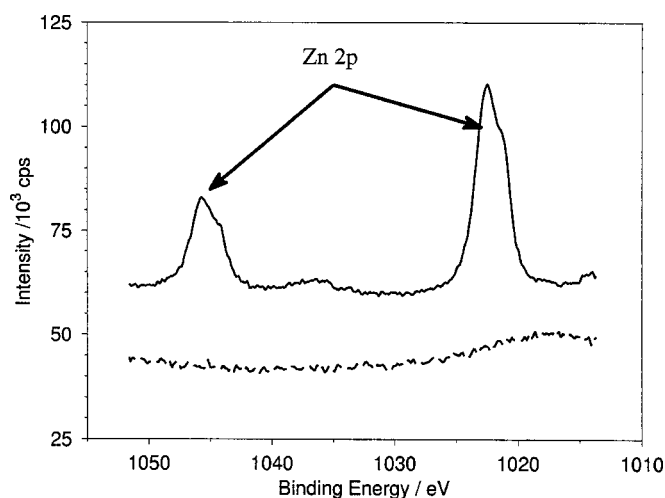


**Figure 7.** XPS analysis of bare platinum (---), offset for clarity, and a platinum electrode conditioned at  $-0.4 \text{ V vs. SCE}$  for 1800 s (—) in 0.1 M  $\text{MgSO}_4$  with 0.02 M  $\text{ZnSO}_4$ , pH 5.0 at 25°C.

exchange to form a 2D alloy did so within 600 s. When the same experiment was repeated using a conditioning potential of 0.2 V vs. SCE, there was no increase in the stripping current in the region of platinum oxidation as shown by the dotted line in Fig. 6. This was interpreted as further evidence that the increase in the stripping current in the region of platinum oxidation was the result of 2D alloy formation and not due to adsorption of a contaminant, since the same contaminant would likely have adsorbed at 0.2 V vs. SCE before being subsequently oxidized in the region of Pt oxidation. As shown in Fig. 7, XPS analysis of a freshly polished platinum electrode subjected to a 30 min conditioning period at  $-0.4 \text{ V vs. SCE}$  in the presence of zinc ions, confirmed the retention of zinc on the electrode surface. The XPS analysis did not contain any peaks attributable to the deposition of inorganic impurities which also verified the purity of the electrolyte.

The effect of conditioning the electrode at  $-0.4 \text{ V vs. SCE}$  on Zn OPD was examined by sweeping the potential into the region of bulk zinc deposition. As illustrated in Fig. 8, there appeared to be a decrease in the nucleation overpotential for Zn OPD, region II, which was also limited to the first 600 s of conditioning. This further

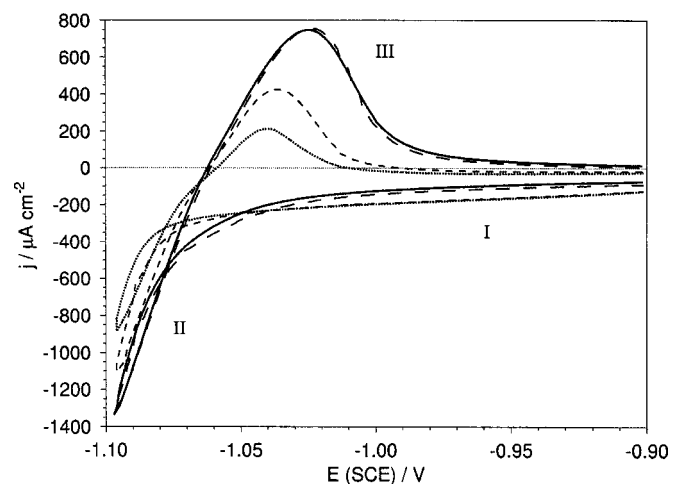


**Figure 8.** Sweep voltammetry of polycrystalline platinum in 0.1 M  $\text{ZnSO}_4$ , pH 4.9 at 25°C, scan rate 20  $\text{mV s}^{-1}$ , 1600 rpm electrode rotation rate, as a function of waiting time at  $-0.4 \text{ V vs. SCE}$ , 0 s (· · · · ·), 120 s (---), 600 s (— · — · —), 1200 s (— — —).

supports the previous assertion of 2D alloy formation. The presence of a contaminant is an unlikely explanation for this observation because such an agent would be liable to block sites for zinc deposition and adversely affect Zn OPD. The rate of hydrogen evolution in region I of Fig. 8 appeared to be diminished upon conditioning. Epelboin *et al.*<sup>27</sup> have proposed an autocatalytic mechanism of zinc electrodeposition from acidic solutions in which zinc adsorption, as  $Zn_{ads}^+$ , competes with hydrogen adsorption,  $H_{ads}$ , as the first step in zinc electrocrystallization. If this model is accepted, the diminished hydrogen evolution would be consistent with enhanced zinc deposition, since hydrogen adsorption precedes hydrogen evolution. These results suggest that hydrogen adsorption on the Zn-Pt alloy is simply not as favorable as on the initially formed UPD Zn layer.

If the electrode was oxidized by sweeping the potential to 1.1 V vs. SCE, then subsequent voltammograms appeared similar to that of the original unconditioned electrode. If on the other hand, after conditioning, the electrode potential was swept back to  $-0.25$  V vs. SCE and then returned to the potential region of zinc deposition, the enhancement of zinc deposition kinetics remained. This potential is significant since it corresponds to the reversible potential for hydrogen evolution from a highly acidic solution of pH *ca.* 0. Thus, by using  $-0.25$  V vs. SCE as the stripping potential to avoid hydrogen evolution, it should be possible to extract current efficiencies for bulk zinc deposition from a wide composition range of acidic zinc sulfate electrolytes by integrating the current-time transients in response to potential steps for zinc deposition and stripping, and calculating the ratio of deposition to stripping charges. However, as mentioned, rapid 3D alloy formation occurring during Zn OPD leads to extreme roughening of the Pt substrate which is visible to the naked eye after extended polarization times. Limiting the Zn OPD polarization times to  $<2$  min was determined to be sufficient for mitigating 3D alloy formation and associated substrate roughening. The real surface area of the electrode, measured from AFM images, after 100 cycles of Zn OPD and stripping increased by only *ca.* 2%. Nevertheless, it is clear that 3D alloy formation can significantly alter the crystallography of the substrate, and this must be kept in mind when performing experiments using single-crystal electrodes.

**Tafel measurements for aqueous zinc sulfate electrolyte solutions.**—The kinetics of zinc deposition from pure zinc sulfate electrolytes, *ca.* pH 4.9 at 25°C, were examined by normal pulse and staircase voltammetry as a function of zinc sulfate concentration, for  $ZnSO_4$  concentration levels of 0.1 mol kg<sup>-1</sup>  $ZnSO_4$ , 0.5 mol kg<sup>-1</sup>  $ZnSO_4$ , and 1.00 mol kg<sup>-1</sup>  $ZnSO_4$ . The current efficiencies for zinc deposition at the disk electrode were always 100% at all applied overpotentials, whether employing the ring-disk electrode to correct the disk current by detecting hydrogen evolution at the ring electrode, or by amperometric integration of the normal potential pulse sequences. The results from staircase voltammetry generally matched well with normal pulse experiments and, hence, were treated as replicates of the same experiment. A typical Tafel plot is shown in Fig. 9 where the solid lines correspond to a fit according to the extended Butler-Volmer equation. The limiting current densities for zinc deposition were calculated using the Levich equation. The diffusion coefficients for  $Zn^{2+}$ ,  $D_{Zn^{2+}}^{\circ}$ , were estimated from the following expression

$$D_{Zn^{2+}} \approx \frac{D_{ZnSO_4}}{2} \left[ 1 + \frac{D_{Zn^{2+}}^{\circ}}{D_{SO_4^{2-}}^{\circ}} \right] = 0.84D_{ZnSO_4} \quad [4]$$

where  $D_{ZnSO_4}$  is the diffusion coefficient for zinc sulfate from the data set of Awakura *et al.*,<sup>28</sup> and  $D_{Zn^{2+}}^{\circ}$  ( $0.703 \times 10^{-9}$  m<sup>2</sup> s<sup>-1</sup>), and  $D_{SO_4^{2-}}^{\circ}$  ( $1.065 \times 10^{-9}$  m<sup>2</sup> s<sup>-1</sup>) are the diffusion coefficients of  $Zn^{2+}$  and  $SO_4^{2-}$  at infinite dilution. The transport number of  $Zn^{2+}$  was fixed at 0.4 (also calculated using the diffusion coefficients of  $Zn^{2+}$

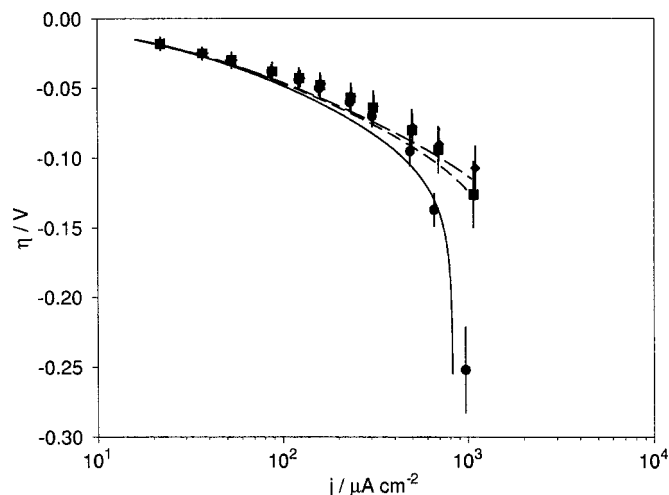


**Figure 9.** Tafel plot for zinc deposition from 0.10 mol kg<sup>-1</sup>  $ZnSO_4$ , pH 4.9 at 25°C, 400 (●), 1600 (■), and 3600 rpm (◆) electrode rotation speed.

and  $SO_4^{2-}$  at infinite dilution) and electrolyte viscosities and densities were calculated using empirical expressions reported by Umetsu *et al.*<sup>29</sup>

Initially, all the data were fit simultaneously to obtain the values for zinc exchange current densities,  $j_{0,Zn}$ , corresponding to each zinc sulfate concentration, as well as a value of the product of the transfer coefficient,  $\alpha$ , and the number of electrons transferred in the rate determining step,  $n$ . The fitting method was a weighted least-squared fit<sup>30</sup> of the differences in the natural logarithms of the observed and calculated current densities, using the inverse of the uncertainty in overpotential as the weighting parameter. Using this method, the best-fit value for  $\alpha n$  was 1.08, which was close to the theoretical value of 1.0 (Tafel slope of 60 mV dec<sup>-1</sup> at 25°C). Due to covariance between the transfer coefficient,  $\alpha$ , and exchange current density,  $j_{0,Zn}$ , a value of 1.0 was adopted for  $\alpha n$  and the corresponding zinc exchange current densities were recalculated to be  $21 \pm 5$  A m<sup>-2</sup>,  $23 \pm 7$  A m<sup>-2</sup>, and  $28 \pm 5$  A m<sup>-2</sup>, for 0.1 mol kg<sup>-1</sup>  $ZnSO_4$ , 0.5 mol kg<sup>-1</sup>  $ZnSO_4$ , and 1.00 mol kg<sup>-1</sup>  $ZnSO_4$ , respectively. These results are plotted in Fig. 10 along with previ-

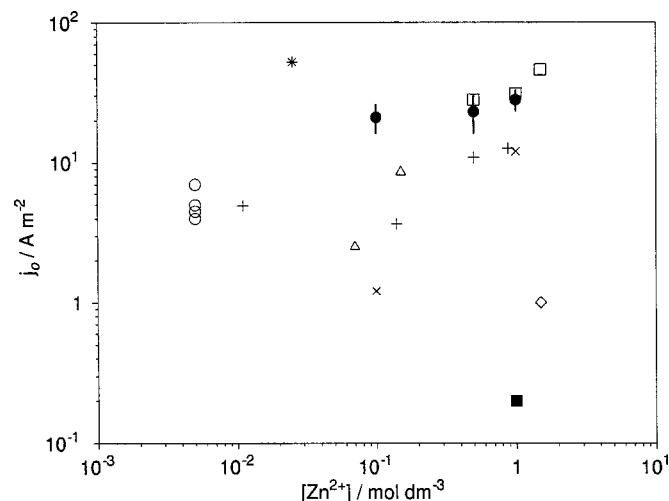


**Figure 10.** Zinc exchange current density in sulphate based electrolytes at 25°C, from (●) this study, (Δ) Zouari and Lapique,<sup>32</sup> (□) Jović *et al.*,<sup>31</sup> (◇) Despić and Pavlović,<sup>14</sup> (○) Hurlen and Brevik,<sup>33</sup> (\*) Budov and Losev,<sup>34</sup> (×) Kahanda and Tomkiewicz,<sup>35</sup> (■) Parsons,<sup>36</sup> and (+) Sierra-Alcazar and Harrison,<sup>37</sup> plotted against zinc concentration.

ously reported zinc exchange current densities in other weakly acidic sulfate electrolytes. Epelboin *et al.*,<sup>27</sup> have reported that addition of even a small amount of acid to a zinc electrolyte causes a shift in the polarization curve to higher cathodic polarizations, *i.e.*, a small concentration of protons in the solution lowers the zinc exchange current density. Thus, the sensitivity of zinc deposition kinetics to acidity probably contributed to the scatter of previously reported zinc exchange current densities in Fig. 10 which were measured in electrolytes with pHs ranging from 3.0 to 6.5. Even so, the exchange current densities measured in this study matched relatively well with those recently reported by Jović *et al.*<sup>31</sup> (pH 3.5) and Zouari and Lapique<sup>32</sup> (pH 4.8) using pure zinc electrodes, confirming the viability of the present methodology.

### Conclusions

The UPD of Zn onto polycrystalline Pt creates a suitable surface on which to study overpotential deposition of zinc. This UPD layer has been characterized in acidic and neutral sulfate solutions using voltammetric charge and XPS measurements. The charge density for UPD Zn deposition on platinum from a neutral sulfate solution was estimated to be  $260 \pm 30 \mu\text{C cm}^{-2}$ , which is in the order of a full monolayer. A decrease in  $\text{H}_2$  evolution rates was also described as evidence of the presence of a Zn UPD layer. The UPD layer was found to evolve into a Zn-Pt alloy when the electrode was polarized at potentials more negative than the UPD potential. The alloy was oxidized at the same potential as the oxidation of Pt, illustrating the small crystallographic misfit and large interaction between Zn and Pt. The alloy also decreased  $\text{H}_2$  evolution rates and enhanced zinc OPD kinetics relative to the freshly deposited UPD layer. The use of Zn UPD on Pt as a substrate for OPD kinetic experiments was determined to yield values for kinetic parameters in agreement with those recently reported using pure Zn electrodes. The application of underpotential deposition, UPD, of the reactive metal onto a noble foreign substrate is proposed as a general method for generating well-defined and reproducible surfaces on which to study overpotential deposition.

### List of Symbols

<i>CPE</i>	constant phase element, $\text{S}^{1/2}$
<i>d</i>	interatomic distance, m
<i>E</i>	electrode potential vs. reference electrode, V
<i>F</i>	crystallographic misfit
<i>F</i>	Faraday constant, $96,485 \text{ C mol}^{-1}$
<i>i</i>	current density, $\text{A m}^{-2}$
<i>i</i> <sub>0</sub>	exchange current density, $\text{A m}^{-2}$
<i>m</i>	molal concentration, $\text{mol kg}^{-1}$
<i>N</i> <sub>A</sub>	Avogadro number, $6.0221367 \times 10^{23} \text{ mol}^{-1}$
<i>R</i> <sub>soln</sub>	solution resistance, $\Omega$
<i>z</i>	charge number

<i>Z</i>	complex impedance, $\Omega$
$\Gamma$	surface concentration, $\text{mol m}^{-2}$
$\xi$	power term of constant phase element
$\omega$	frequency, $\text{rad s}^{-1}$

### References

1. R. de Levie, *J. Electroanal. Chem.*, **281**, 1 (1990).
2. E. Budevski, G. Staikov, and W. J. Lorenz, *Electrochim. Acta*, **45**, 2559 (2000).
3. E. Budevski, G. Staikov, and W. J. Lorenz, *Electrochemical Phase Formation and Growth: An Introduction to the Initial Stages of Metal Deposition*, VCH Publishers, New York (1996).
4. W. Lehnert and W. Schmickler, *J. Electroanal. Chem.*, **310**, 27 (1991).
5. C. Sanchez and E. Leiva, *J. Electroanal. Chem.*, **458**, 183 (1998).
6. A. Aramata, Md. A. Quaiyyum, W. A. Balais, T. Atoguchi, and M. Enyo, *J. Electroanal. Chem.*, **338**, 367 (1992).
7. Md. A. Quaiyyum, A. Aramata, S. Moniwa, S. Taguchi, and M. Enyo, *J. Electroanal. Chem.*, **373**, 61 (1994).
8. S. Taguchi and A. Aramata, *J. Electroanal. Chem.*, **396**, 131 (1995).
9. A. Aramata, S. Terui, S. Taguchi, T. Kawaguchi, and K. Shimazu, *Electrochim. Acta*, **41**, 761 (1996).
10. G. Horányi and A. Aramata, *J. Electroanal. Chem.*, **434**, 201 (1997).
11. A. Aramata, S. Taguchi, T. Fukuda, M. Nakamura, and G. Horányi, *Electrochim. Acta*, **44**, 999 (1998).
12. S. Taguchi and A. Aramata, *J. Electroanal. Chem.*, **457**, 73 (1998).
13. K. Igarashi, A. Aramata, and S. Taguchi, *Electrochim. Acta*, **46**, 1773 (2001).
14. A. R. Despić and M. G. Pavlović, *Electrochim. Acta*, **27**, 1539 (1982).
15. A. Tadjeddine, M. Ladouceur, A. Lahrichi, D. Guay, and G. Tourillon, in *X-Ray Methods in Corrosion and Interfacial Electrochemistry*, A. J. Davenport and J. G. Gordon, Editors, PV 92-1, p. 159, The Electrochemical Society Proceedings Series, Pennington, NJ (1992).
16. H. J. Pauling, G. Staikov, and K. Jüttner, *J. Electroanal. Chem.*, **376**, 179 (1994).
17. U. Schmidt, S. Vinzelberg, and G. Staikov, *Surf. Sci.*, **348**, 261 (1996).
18. V. D. Jović and B. M. Jović, *Electrochim. Acta*, **47**, 1777 (2002).
19. R. Vindu and S. Hara, *J. Electroanal. Chem.*, **475**, 171 (1999).
20. G. Inzelt and G. Horányi, *J. Electroanal. Chem.*, **491**, 111 (2000).
21. D. Carnal, P. I. Oden, U. Müller, E. Schmidt, and H. Siegenthaler, *Electrochim. Acta*, **40**, 1223 (1995).
22. J. W. Yan, H. Tang, Y. Y. Yang, J. W. Wu, Z. X. Xie, S. G. Sun, and B. W. Mao, *Surf. Interface Anal.*, **32**, 49 (2001).
23. H. H. Uhlig, J. S. MacNaim, and D. A. Vagn, *Acta Metall.*, **3**, 302 (1955).
24. A. Lachenwitzet, N. Li, and J. Lipkowski, *J. Electroanal. Chem.*, **532**, 85 (2002).
25. S. Swathirajan and S. Bruckenstein, *J. Electrochem. Soc.*, **129**, 1202 (1982).
26. H. Mascaro-Lucia, M. C. Santos, S. A. S. Machado, and L. A. Avaca, *J. Braz. Chem. Soc.*, **13**, 529 (2002).
27. I. Epelboin, M. Ksouri, and R. Wiert, *J. Electrochem. Soc.*, **122**, 1206 (1975).
28. Y. Awakura, T. Doi, and T. H. Majima, *Metall. Mater. Trans. B*, **19**, 5 (1988).
29. Y. Umetsu, Q. Su, and K. Tozawa, *Shigen to Kankya*, **104**, 829 (1988).
30. D. C. Montgomery, *Design and Analysis of Experiments*, 4th ed., John Wiley & Sons, Inc., New York (1997).
31. V. D. Jović, J. N. Jovićević, M. G. Pavlović, and R. M. Stevanović, *J. Serb. Chem. Soc.*, **55**, 341 (1990).
32. I. Zouari and F. Lapique, *Electrochim. Acta*, **37**, 439 (1992).
33. T. Hurlen and T. R. Breivik, *Acta Chem. Scand.*, **32**, 447 (1961).
34. G. M. Budov and V. V. Losev, *Russ. J. Phys. Chem.*, **37**, 784 (1963).
35. G. L. M. K. S. Kahanda and M. Tomkiewicz, *J. Electrochem. Soc.*, **136**, 1497 (1989).
36. R. Parsons, *Handbook of Electrochemical Constants*, Butterworths, London (1959).
37. H. B. Sierra-Alcazar and J. A. Harrison, *Electrochim. Acta*, **22**, 627 (1977).